Chem Soc Rev

REVIEW ARTICLE

View Article Online
View Journal | View Issue

Garnet-type solid-state fast Li ion conductors for Li batteries: critical review

Cite this: *Chem. Soc. Rev.*, 2014, **43**, 4714

Venkataraman Thangadurai,* Sumaletha Narayanan and Dana Pinzaru

Batteries are electrochemical devices that store electrical energy in the form of chemical energy. Among known batteries, Li ion batteries (LiBs) provide the highest gravimetric and volumetric energy densities, making them ideal candidates for use in portable electronics and plug-in hybrid and electric vehicles. Conventional LiBs use an organic polymer electrolyte, which exhibits several safety issues including leakage, poor chemical stability and flammability. The use of a solid-state (ceramic) electrolyte to produce all-solid-state LiBs can overcome all of the above issues. Also, solid-state Li batteries can operate at high voltage, thus, producing high power density. Various types of solid Li-ion electrolytes have been reported; this review is focused on the most promising solid Li-ion electrolytes based on garnet-type metal oxides. The first studied Li-stuffed garnet-type compounds are $Li_5La_3M_2O_{12}$ (M = Nb, Ta), which show a Li-ion conductivity of $\sim 10^{-6}$ at 25 °C. La and M sites can be substituted by various metal ions leading to Li-rich garnet-type electrolytes, such as $Li_6ALa_2M_2O_{12}$, (A = Mg, Ca, Sr, Ba, $Sr_{0.5}Ba_{0.5}$) and $Li_7La_3C_2O_{12}$ (C = Zr, Sn). Among the known Li-stuffed garnets, $Li_{6.4}La_3Zr_{1.4}Ta_{0.6}O_{12}$ exhibits the highest bulk Li-ion conductivity of 10^{-3} S cm^{-1} at 25 °C with an activation energy of 0.35 eV, which is an order of magnitude lower than that of the currently used polymer, but is chemically stable at higher temperatures and voltages compared to polymer electrolytes. Here, we discuss the chemical composition–structure–ionic conductivity relationship of the Li-stuffed garnet-type oxides, as well as the Li ion conduction mechanism.

Received 13th January 2014

DOI: 10.1039/c4cs00020j

www.rsc.org/csr

Department of Chemistry, University of Calgary, 2500 University Dr NW, Calgary, AB, T2N 1N4, Canada. E-mail: vthangad@ucalgary.ca; Tel: +1 403 210 8649

Venkataraman Thangadurai

Dr Venkataraman Thangadurai is an Associate Professor of Chemistry and Associate Director of CAESR (Calgary Advanced Energy Storage and Conversion Research) at the University of Calgary. He received his PhD from the Indian Institute of Science (IISc), Bangalore, India and subsequently completed his postdoctoral research from the University of Kiel, Germany. He was awarded with the prestigious postdoctoral research fellowship from the Alexander von Humboldt (AvH) Foundation, Bonn, Germany. He also received his Habilitation degree from the University of Kiel. He was a visiting Associate Professor at the University of Maryland, College Park, USA. His present research activities include developing novel solid electrolytes and electrodes for energy conversion and storage devices, including solid oxide fuel cells (SOFCs), proton conducting solid oxide fuel cells (H-SOFCs), all-solid-state Li ion batteries, as well as electrochemical gas sensors.

Sumaletha Narayanan

Sumaletha Narayanan is pursuing her PhD degree in Chemistry under the guidance of Dr V. Thangadurai at the University of Calgary. She received her BSc and MSc in Chemistry from Calicut University, and Bharathiar University in India, respectively. She worked as a project assistant with Dr K. G. K. Warrier in the Ceramic Technology Division at the National Institute for Interdisciplinary Science and Technology, Trivandrum, India (2007–2009). She joined Thangadurai's group in 2009 and obtained her second Masters, in the area of garnet-like electrolytes for Li ion batteries, in 2012. Her primary research interest involves developing solid-state electrolytes for all-solid-state Li ion batteries and proton exchange membrane fuel cells.

1. Introduction

With the expected decline in conventional fossil fuels, recently there has been growing interest in developing technologies for alternative green (zero emissions) energy storage and conversion devices such as batteries, fuel cells, and solar cells for transportation, stationary power and distributed power generation applications. Unlike fuel cells, which require a constant supply of fuels and oxidants, batteries can be completely self-contained and require no chemical input or export. Like other electrochemical devices, batteries also consist of an electrolyte, which allows the transfer of ions from the negative (anode) to the positive (cathode) during discharge, facilitating the movement of electrons through an external circuit. During charging, the ions move in an opposing fashion, and the use of electrical energy pushes the electrons and Li ions back to the anode. Among the known batteries, so far, Li-ion batteries exhibit the highest volumetric and gravimetric energy densities.[1]

Elemental Li is the lightest and the most electropositive element, thus offering the highest cell voltage. The predominant anode and cathode materials used in LiBs are graphitic C and $LiCoO_2$, respectively. These materials show poor cyclic performances, low energy density, and they form reaction products at the electrolyte and electrode interfaces during the operation of the battery. The current Li ion electrolytes, for example, $LiBF_4$, $LiPF_6$, and $LiCF_3SO_3$ dissolved in organic solvents such as ethylene carbonate, propylene carbonate, polyethylene oxide and dimethyl carbonate, which are flammable, have poor electrochemical stability and a limited temperature range of operation, exhibit leakage, and pose health hazards.[1] Hence, the use of solid-state (ceramic) electrolytes has been proposed for the development of safe LiBs due to their desired physical and chemical properties which provide higher power density compared to the conventional polymer electrolyte based LiBs.

1.1 Solid-state (ceramic) Li ion electrolytes

Solid-state Li ion electrolytes are being considered to replace organic polymer-based electrolytes with the advantages of miniaturization for portable electronic devices and chemical stability at higher temperatures, while being non-reactive towards an ambient atmosphere. The key functional properties sought after in a solid electrolyte include:

- high total (bulk + grain-boundary) Li-ion conductivity of about 10^{-2} S cm^{-1} with the Li ion transference number close to unity ($t_{Li+} \sim 1$) at the Li activities of anode and cathode in LiBs;
- chemical stability with high voltage Li cathodes and a high electrochemical decomposition voltage of $\sim$6 V *versus* elemental Li and Li alloy anode;
- chemical stability against reaction with the anode or cathode during LiB manufacture and operation in order to prevent formation of any undesired side reaction products at the electrode–electrolyte interfaces;
- negligible solid-state electrode–electrolyte interface charge-transfer resistance; and
- amenable to inexpensive and environmentally friendly thin-film preparation methods.[2–4]

A large number of inorganic oxides and non-oxides exhibiting amorphous and crystalline structures have been investigated.[2–5] Fig. 1 shows the idealized crystal structures of most studied solid-state Li ion electrolyte materials, including NASICON (sodium super ionic conductors)-type phosphates, perovskite-type $La_{(2/3)-x}Li_{3x}TiO_3$ (LLT), Li-β-alumina, Li_3N, and Li_4SiO_4. Among them, LLT exhibits the highest bulk conductivity of $\sim 10^{-3}$ S cm^{-1}, but LLT-based electrolytes have a distinct drawback of poor electrochemical and chemical stability with elemental Li and Li alloy.[5] They also exhibit very large grain-boundary impedance to total conductivity, especially at low temperature. Another highly conductive and Li metal stable Li-ion electrolyte, Li_3N, also has the problem of a low decomposition voltage of 0.44 V at room temperature. Layered-structured Li-β-alumina shows isotropic conductivity and is sensitive to moisture and carbon dioxide.[2–5]

Recently discovered garnet-type materials,[6–8] $Li_5La_3M_2O_{12}$ (M = Nb, Ta), in the Li_2O–La_2O_3–M_2O_5 (M = Nb or Ta) system provide a high total (bulk + grain-boundary) conductivity of 10^{-6} S cm^{-1} at room temperature. Garnet-type structure derived materials exhibit several desired physical and chemical properties; hence, being considered for all-solid state LiBs.[6–8] Fig. 2 shows the number of papers reported on Li ion conducting garnet-type metal oxides since 2003. In 2010, Cussen reviewed the crystal structure and Li ion transport properties of Li-stuffed garnet-type oxides,[9] thus, the present review work is mainly focused on the chemical composition–ionic conductivity relationship, together with the mechanism of Li ion conduction.

Dana Pinzaru

Dana Pinzaru was born and raised in the city of Bacau, Romania. She moved to Calgary, Canada in 2005, at the age of 16. She is currently pursuing her MSc degree at the University of Calgary under the supervision of Dr V. Thangadurai. She obtained her bachelor's degree in Chemistry from the University of Calgary in 2012. Her current research is focused on developing garnet-like solid Li ion electrolytes for all-solid-state Li ion batteries.

2. Garnet and Li stuffed garnet-type structures

The ideal garnets exhibit a general chemical formula of $A_3B_2(XO_4)_3$ (A = Ca, Mg, Y, La or rare earth; B = Al, Fe, Ga, Ge, Mn, Ni or V; X = Si, Ge, Al) where A, B and C are eight, six and four oxygen coordinated cation sites, which crystallize in a face centered cubic structure with the space group $Ia\bar{3}d$.[10] Fig. 3a shows the structure of ideal garnet-type metal oxides. They exhibit very useful technologically related physical and chemical

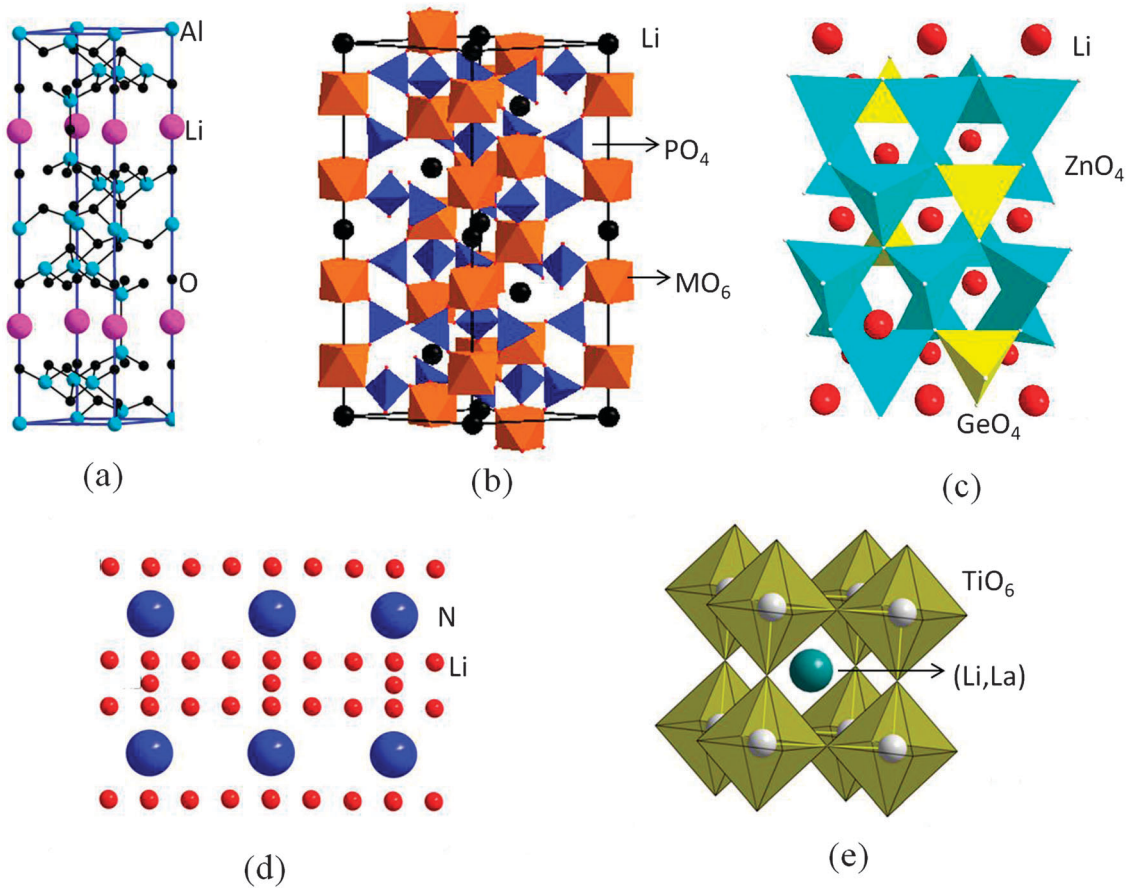

Fig. 1 Idealized crystal structure for solid-state Li ion conductors, (a) Li-β-alumina, (b) sodium super ion conducting (NASICON) phosphate $LiM_2(PO_4)_3$ (M = Ti, Zr), (c) lithium superior conducting (LISICON) $Li_3Zn_{0.5}GeO_4$, (d) Li_3N and (e) A-site deficient perovskite-type $La_{(2/3)-x}Li_{3x}TiO_3$. Structure-type (a) and (d) show the isotropic Li ion conduction while all other members exhibit anisotropic Li ion conduction.

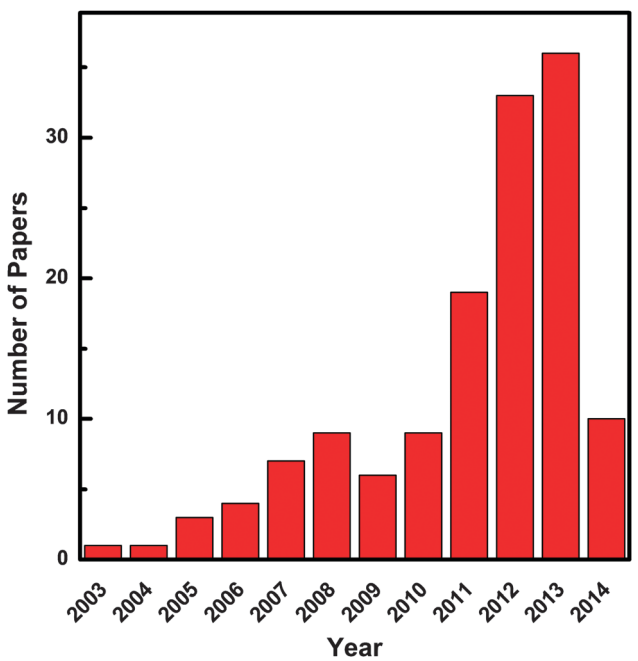

Fig. 2 Number of papers published since 2003 on Li-stuffed garnets (accessed web of science on February 28, 2014).

properties, which make them ideal materials for magnetic and optical devices. Another unique and perhaps the most important, but rather uncommon characteristic of Li-excess garnet-type materials is ionic conduction. Commonly studied garnets typically contain five to seven Li atoms per formula unit, and are referred to as Li-stuffed (Li-rich) garnets, that is, they have more Li than that can be accommodated at the tetrahedral sites, leaving excess Li which occupy the octahedral sites in the garnet structure.[9]

The first reported Li ion conducting Li-stuffed garnets are $Li_5La_3M_2O_{12}$ (M = Nb, Ta), which were developed by Thangadurai *et al.* in 2003.[8] Fig. 3b shows the idealized crystal structure of $Li_5La_3M_2O_{12}$. Synthesis of these compounds has been attempted many times since, and has consistently shown the same conductivity of $\sim 10^{-6}$ at 25 °C and good chemical stability at a wide range of operating temperatures. La and M sites can be substituted by various metal ions leading to Li-rich garnet-type $Li_6ALa_2M_2O_{12}$ (A = Mg, Ca, Sr, Ba, $Sr_{0.5}Ba_{0.5}$) and $Li_7La_3C_2O_{12}$, (C = Zr, Sn) and $Li_7La_3Ta_2O_{13}$.[9,11–19] Further research has since been done to understand the crystal structure, electrical conductivity, and the mechanism of Li ion conduction. Attempts have also been made to incorporate these materials in an all-solid-state LiBs. In the following sections, we briefly

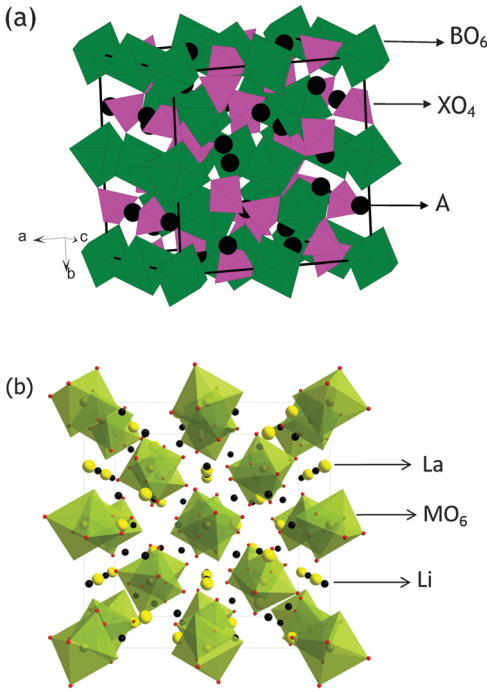

Fig. 3 Idealized crystal structure of (a) garnet and (b) garnet-related $Li_5La_3M_2O_{12}$, showing the polyhedral connectivity of Li, La, and MO_6 in the Li-stuffed garnets.

discuss the chemical composition–structure relationship of the Li stuffed garnet-type oxides.

2.1 $Li_3Ln_3Te_2O_{12}$ (Ln = Y, Pr, Nd, Sm–Lu) (Li_3-phases) and $Li_{3+x}Nd_3Te_{2-x}Sb_xO_{12}$ (x = 0.05–1.5)

O'Callaghan *et al.* developed garnet-type $Li_3Ln_3Te_2O_{12}$ (Ln = Y, Pr, Nd, Sm–Lu) to investigate the relationship between Li site occupation and Li ion conductivity.[20] Table 1 lists the cell constant, final sintering temperature, and conductivity of some of the members of $Li_3Ln_3Te_2O_{12}$ together with other known Li-stuffed garnet-type metal oxides.[8,11–66] The lattice constant increases with increasing Ln ionic radius in $Li_3Ln_3Te_2O_{12}$. In $Li_3Ln_3Te_2O_{12}$, Li ions are located exclusively in the tetrahedral (24d) sites in the space group $Ia\bar{3}d$. These $Li_3Ln_3Te_2O_{12}$ garnets have exhibited a fairly low ionic conductivity of $\sim 10^{-5}$ S cm^{-1} at 600 °C with a high activation energy (>1 eV),[21] suggesting that Li in the tetrahedral sites are less mobile and, ultimately, they seem not to be responsible for the high Li ion conduction in the Li-stuffed garnets $Li_5La_3M_2O_{12}$, $Li_6ALa_2M_2O_{12}$ and $Li_7La_3Zr_2O_{12}$.[12,13,16,18,28,43,44] To increase the ionic conductivity, the goal would be to optimize the amount of Li present in the octahedral sites in the garnet-type structure. Subsequently, O'Callaghan *et al.* prepared Li-excess $Li_{3+x}Nd_3Te_{2-x}Sb_xO_{12}$ (x = 0.05–1.5), with lattice parameters ranging from 12.55576(12) Å for x = 0.05 to 12.6253(2) Å for x = 1.5.[22] They found that the Li ion conductivity increased with increasing Li content, reaching a value of $\sim 10^{-2}$ S cm^{-1} at 400 °C for $Li_{3.5}Nd_3Te_{1.5}Sb_{0.5}O_{12}$.[22]

2.2 $Li_5La_3M_2O_{12}$ (M = Nb, Ta, Sb) (Li_5-phases)

The exact crystal structure of the first reported garnet-type $Li_5La_3M_2O_{12}$ has been quite controversial, particularly for the occupation of the Li ions. The Mazza group first proposed the garnet-type structure with a space group $Ia\bar{3}d$, similar to that of the ideal garnet-structure, for $Li_5La_3M_2O_{12}$ in 1988.[6] However, Hyooma and Hayashi suggested a space group $I2_13$, which was non-centrosymmetric and less symmetric, from single-crystal X-ray diffraction (XRD).[7] Using neutron diffraction (ND), for the first time, Cussen confirmed that $Li_5La_3M_2O_{12}$ crystallizes in a space group $Ia\bar{3}d$, similar to the Mazza model, with the excess Li^+ ions being distributed over tetrahedral (24d) as well as distorted octahedral sites (96h/48g). In $Li_5La_3M_2O_{12}$, excess Li exists, compared to the ideal garnet structure that could not all be incorporated into the ideal garnets tetrahedral sites, thus, the excess Li is incorporated into the octahedral sites in the Li-rich garnets.[23] Both of these sites are partially filled in $Li_5La_3M_2O_{12}$.[23] Nb/Ta in $Li_5La_3M_2O_{12}$ has been fully replaced or partially doped, including Bi,[24,25] Sb[26,27] and In[28] and La with Pr, Nd,[29] Ba[30] and K.[28] It has been shown that the presence of d^{10} (for *e.g.*, Te^{6+}, Sb^{5+}) cations, rather than d^0 (for *e.g.*, W^{6+}, Ta^{5+}, Nb^{5+}) cations in the M site, results in an increase in the lattice parameter (Table 1).[20,27]

2.3 $Li_6ALa_2M_2O_{12}$ (A = Mg, Ca, Sr, Ba; M = Nb, Ta) (Li_6-phases)

Further garnet-like structures have been obtained by partially substituting the trivalent La^{3+} with divalent ions, which resulted in an increased Li ion concentration, producing a new class of garnet-type metal oxides with chemical formula of $Li_6ALa_2M_2O_{12}$ (A = Mg, Ca, Sr, Ba, $Sr_{0.5}Ba_{0.5}$ and M = Nb, Ta) (Table 1).[11–19] Many attempts have been made in the past to explain the location of the excess Li^+ ions in the structure using powder X-ray diffraction (PXRD) and ND. However, the attempts using PXRD have yielded many different claims about the possible Li sites in the structure. This is because the Li^+ ion has a very weak XRD scattering factor. ND studies have provided good explanations about the proposed locations of the Li^+ ions in the garnet-type structure. Awaka *et al.* proposed that, compared to the Li_3-garnet model where the Li^+ ions solely occupy the tetrahedral sites (24d), Li^+ ions in the Li_6-phases occupy both tetrahedral (24d) sites (Li(1)) and distorted octahedral (96h) sites (Li(2)). The Li(1)–O distance in $Li_6ALa_2Ta_2O_{12}$ (A = Ca, Ba) was found to be 1.867(5) Å for A = Ca and 1.935(5) Å for A = Ba, while the Li(2)–O distances were found to be in the range of 2.57(5) Å–2.68(4) Å for $Li_6CaLa_2Ta_2O_{12}$ and 2.75(4) Å–2.78(4) Å for $Li_6BaLa_2Ta_2O_{12}$.[14]

Substitution of La^{3+} with the divalent ions and tri- and tetravalent ions for pentavalent Nb/Ta ions resulted in increased occupancy of the Li(2) sites and decreased occupancy of the Li(1) sites, therefore, the concentration of the vacancies on the tetrahedral (24d) sites increased and the concentration of vacancies on the octahedral (96h/48g) sites decreased in the Li_6 phases compared to Li_5 phases. The large number of vacancies in these Li-rich compounds allow for clustering of the Li ions to avoid electrostatic repulsion caused by small Li–Li distances within the structure. As a result, Li ion displacements are observed on the distorted octahedral site (48g).[67] Structurally, the tetrahedra are linked to the octahedra in such a fashion that each octahedron is connected to 2 tetrahedra, while each

Table 1 Chemical composition, synthesis temperature, lattice parameter, and Li ion conductivity of garnets reported in the literature

Compound	Unit cell (Å)	σ_{Li^+} (T °C) (S cm^{-1})	E_a (eV)	Ref.
$Li_3Nd_3Te_2O_{12}$ (850 °C)	12.56253(9)	1.0×10^{-5} (600 °C/air)	1.22	20
$Li_3Gd_3Te_2O_{12}$ (900 °C)	12.3792(1)	8.8×10^{-7} (450 °C/air)	0.88	21
$Li_3Tb_3Te_2O_{12}$ (900 °C)	12.35578(9)	4.4×10^{-6} (450 °C/air)	0.77	21
$Li_3Er_3Te_2O_{12}$ (900 °C)	12.22712(9)	2.8×10^{-8} (450 °C/air)	1.21	21
$Li_3Lu_3Te_2O_{12}$ (900 °C)	12.15970(14)	8.1×10^{-8} (450 °C/air)	~1.2	21
$Li_{3+x}Nd_3Te_{2-x}Sb_xO_{12}$				
x = 0.05 (960 °C)	12.55576(12)	$\sim 3 \times 10^{-5}$ (400 °C/air)	~0.67	22
x = 0.10 (960 °C)	12.5597(9)	$\sim 2 \times 10^{-4}$ (400 °C/air)	~0.56	22
x = 0.20 (960 °C)	12.5602(2)	$\sim 3 \times 10^{-4}$ (400 °C/air)	~0.50	22
x = 0.50 (960 °C)	12.59413(12)	$\sim 1 \times 10^{-2}$ (400 °C/air)	~0.56	22
x = 1.00 (960 °C)	12.62138(12)	$\sim 4 \times 10^{-3}$ (400 °C/air)	~0.63	22
x = 1.50 (960 °C)	12.6253(2)	$\sim 3 \times 10^{-3}$ (400 °C/air)	~0.59	22
$Li_{5+x}BaLa_2Ta_2O_{11.5+0.5x}$				
x = 0.50 (900 °C)	~12.94	3.55×10^{-5} (50 °C/air)	0.47	30
x = 0.75 (900 °C)	~12.96	9.48×10^{-5} (50 °C/air)	0.44	30
x = 1.00 (900 °C)	~12.98	1.81×10^{-4} (50 °C/air)	0.42	30
x = 1.25 (900 °C)	~12.96	1.57×10^{-4} (50 °C/air)	0.42	30
x = 1.50 (900 °C)	~12.96	1.07×10^{-4} (50 °C/air)	0.42	30
x = 1.75 (900 °C)	~12.95	1.09×10^{-4} (50 °C/air)	0.42	30
x = 2.00 (900 °C)	~12.95	1.01×10^{-4} (50 °C/air)	0.45	30
$Li_5La_3Nb_2O_{12}$ (900 °C, sol–gel method)	12.805	1.0×10^{-5} (22 °C/air)	0.43	32
$Li_5La_3Nb_2O_{12}$ (950 °C)	12.762(3)	8.0×10^{-6} (50 °C/air)	0.43	8
$Li_5La_3Nb_2O_{12}$ (950 °C)	12.8189(9)	2.3×10^{-5} (50 °C/air)	0.55	28
$Li_5La_3Nb_2O_{12}$ (1100 °C)	12.718(2)	5.08×10^{-6} (22 °C/air)	0.60	33
$Li_5La_3Ta_2O_{12}$ (900 °C, sol–gel method)	12.85	1.54×10^{-6} (25 °C/air)	0.57	34
$Li_5La_3Ta_2O_{12}$ (950 °C)	12.766(3)	1.2×10^{-6} (25 °C/air)	0.56	8
$Li_5La_3Ta_2O_{12}$ (1200 °C)	—	3.9×10^{-4} (25 °C/air)	—	35
$Li_5La_3Sb_2O_{12}$ (950 °C)	12.8566(18)	8.2×10^{-6} (24 °C/Ar)	0.51	26
$Li_5La_3Sb_2O_{12}$ (950 °C)	12.8518(3)	—	—	27
$Li_5La_3Bi_2O_{12}$ (775 °C)	13.0652(4)	4.0×10^{-5} (22 °C/Ar)	0.47	24
$Li_5La_3Bi_2O_{12}$ (650 °C, Pechini sol–gel method)	13.06(5)	2.4×10^{-5} (24 °C/air)	0.40	25
$Li_5Nd_3Ta_2O_{12}$ (Flux synthesis)	12.5967(1)	$\sim 1 \times 10^{-8}$ (300 °C/air)	—	29
$Li_5Nd_3Sb_2O_{12}$ (925 °C)	12.66238(3)	1.3×10^{-7} (25 °C/air)	0.67	31
$Li_5La_3Nb_{2-x}Y_xO_{12-\delta}$				
x = 0.05 (1100 °C)	12.717 (2)	1.34×10^{-5} (23 °C/air)	0.45	33
x = 0.10 (1100 °C)	12.717(3)	1.44×10^{-5} (23 °C/air)	0.51	33
x = 0.15 (1100 °C)	12.732(9)	5.71×10^{-5} (25 °C/air)	0.43	33
x = 0.20 (1100 °C)	12.743(8)	9.13×10^{-5} (23 °C/air)	0.43	33
x = 0.25 (1100 °C)	12.717(5)	9.68×10^{-5} (23 °C/air)	0.43	33
$Li_{5.5}La_3Nb_{1.75}In_{0.25}O_{12}$ (950 °C)	12.821(2)	1.8×10^{-4} (50 °C/air)	0.51	28
$Li_{5.5}La_{2.75}K_{0.25}Nb_2O_{12}$ (950 °C)	12.7937(8)	6.0×10^{-5} (50 °C/air)	0.49	28
$Li_{5.5}La_3Zr_2Ga_{0.5}O_{12}$ (1000 °C)	12.9697(1)	1×10^{-4} (23 °C/air)	—	36
$Li_6MgLa_2Ta_2O_{12}$ (900 °C)	12.794(1)	2.74×10^{-6} (50 °C/Ar)	—	11
$Li_6MgLa_2Ta_2O_{12}$ (950 °C)	12.802(2)	2.67×10^{-6} (50 °C/Ar)	0.51	11
$Li_6CaLa_2Nb_2O_{12}$ (900 °C)	12.697(2)	1.6×10^{-6} (22 °C/air)	0.55	12
$Li_6CaLa_2Ta_2O_{12}$ (900 °C)	12.719(1)	2.65×10^{-6} (50 °C/Ar)	—	11
$Li_6CaLa_2Ta_2O_{12}$ (950 °C)	12.734(3)	3.59×10^{-6} (50 °C/Ar)	0.53	11
$Li_6CaLa_2Ta_2O_{12}$ (1000 °C)	12.725(2)	2.2×10^{-6} (27 °C/air)	0.50	14
$Li_6BaLa_2Nb_2O_{12}$ (900 °C)	12.868(1)	6×10^{-6} (22 °C/air)	0.44	12
$Li_6BaLa_2Nb_2O_{12}$ (900 °C)	12.8893(2)	6.69×10^{-6} (22 °C/air)	0.42	37
$Li_6BaLa_2Nb_{0.5}Ta_{1.5}O_{12}$ (900 °C)	12.87876(6)	4.21×10^{-6} (25 °C/air)	0.47	37
$Li_6BaLa_2NbTaO_{12}$ (900 °C)	12.9897(5)	3.09×10^{-6} (25 °C/air)	0.47	37
$Li_6BaLa_2Nb_{1.5}Ta_{0.5}O_{12}$ (900 °C)	13.0681(2)	1.06×10^{-6} (25 °C/air)	0.50	37
$Li_6BaLa_2Ta_2O_{12}$ (850 °C Pechini sol–gel method)	12.995(2)	1.69×10^{-5} (25 °C/air)	0.40	38
$Li_6BaLa_2Ta_2O_{12}$ (900 °C)	12.946(3)	5.38×10^{-5} (22 °C/air)	0.40	13
$Li_6BaLa_2Ta_2O_{12}$ (900 °C)	12.9958(9)	8.77×10^{-6} (25 °C/air)	0.41	37
$Li_6BaLa_2Ta_2O_{12}$ (900 °C)	12.973	1.30×10^{-4} (50 °C/Ar)	—	11
$Li_6BaLa_2Ta_2O_{12}$ (950 °C)	12.975	1.01×10^{-4} (50 °C/Ar)	0.42	11
$Li_6BaLa_2Ta_2O_{12}$ (1000 °C)	13.001(4)	1.3×10^{-5} (25 °C/air)	0.44	14
$Li_6La_3SnSbO_{12}$ (1130 °C)	12.8991	2.2×10^{-5} (20 °C/air)	0.504	15
$Li_6La_3SnNbO_{12}$ (1130 °C)	12.8682	3.5×10^{-5} (20 °C/air)	0.503	15
$Li_6La_3SnTaO_{12}$ (1130 °C)	12.8693	4.2×10^{-5} (20 °C/air)	0.498	15
$Li_6SrLa_2Nb_2O_{12}$ (900 °C)	12.811(1)	4.2×10^{-6} (22 °C/air)	0.50	12
$Li_6SrLa_2Ta_2O_{12}$ (900 °C)	12.808(2)	8.84×10^{-6} (22 °C/air)	0.50	13
$Li_6SrLa_2Ta_2O_{12}$ (900 °C)	12.826	2.61×10^{-5} (50 °C/Ar)	—	11
$Li_6SrLa_2Ta_2O_{12}$ (950 °C)	12.835	3.66×10^{-5} (50 °C/Ar)	0.45	11
$Li_6Sr_{0.5}Ba_{0.5}La_2Ta_2O_{12}$ (900 °C)	12.879	4.64×10^{-5} (50 °C/Ar)	—	11
$Li_6Sr_{0.5}Ba_{0.5}La_2Ta_2O_{12}$ (950 °C)	12.862	4.96×10^{-5} (50 °C/Ar)	0.44	11
$Li_6SrLa_2Sb_2O_{12}$ (950 °C)	12.8933(3)	6.6×10^{-6} (24 °C/Ar)	0.54	26
$Li_6CaLa_2Sb_2O_{12}$ (900 °C)	12.78594(12)	1.0×10^{-7} (95 °C/air)	0.82(3)	21

Table 1 (*continued*)

Compound	Unit cell (Å)	σ_{Li^+} (T °C) (S cm^{-1})	E_a (eV)	Ref.
$Li_6SrLa_2Bi_2O_{12}$ (750 °C)	13.0893(9)	5.2×10^{-5} (22 °C/Ar)	0.42	24
$Li_6La_3ZrTaO_{12}$ (1120 °C)	12.8873	2.5×10^{-4} (25 °C/air)	0.42	39
$Li_6La_3Zr_{1.5}W_{0.5}O_{12}$ (1100 °C)	12.94385	2.08×10^{-4} (30 °C/air)	0.46	40
$Li_{6.15}La_3Zr_{1.75}Ta_{0.25}Al_{0.2}O_{12}$ (1050 °C co-precipitation and hot pressing method)	12.95	0.37×10^{-3} (25 °C/air)	0.30	41
$Li_{6.15}La_3Zr_{1.75}Ta_{0.25}Ga_{0.2}O_{12}$ (1050 °C co-precipitation and hot pressing method)	12.95	0.41×10^{-3} (25 °C/air)	0.27	41
$Li_{6.25}La_3Zr_2Ga_{0.25}O_{12}$ (1000 °C co-precipitation and hot pressing method)	12.9710(5)	3.5×10^{-4} (23 °C/air)	—	42
$Li_{6.4}La_3Zr_{1.4}Ta_{0.6}O_{12}$ (1140 °C)	12.923	1.0×10^{-3} (25 °C/air)	0.35	43
$Li_{6.4}La_3Zr_{1.7}W_{0.3}O_{12}$ (1100 °C)	12.96507	7.89×10^{-4} (30 °C/air)	0.45	40
$Li_{6.5}La_{2.5}Ba_{0.5}ZrNbO_{12}$ (1100 °C)	12.815(4)	—	0.31	44
$Li_{6.5}La_{2.5}Ba_{0.5}ZrTaO_{12}$ (1100 °C)	12.783(4)	2.00×10^{-4} (23 °C/air)	0.31	44
$Li_{6.5}La_{2.5}Ba_{0.5}ZrTaO_{12}$ (1100 °C)	12.764(3)	8.76×10^{-5} (24 °C/air)	0.34	45
$Li_{6.5}La_3Zr_{1.75}Te_{0.25}O_{12}$ (1100 °C)	12.9134	1.02×10^{-3} (30 °C/air)	0.38	46
$Li_{6.5}La_3Nb_{1.25}Y_{0.75}O_{12}$ (1100 °C)	12.9488(11)	2.7×10^{-4} (30 °C/air)	0.36	47
$Li_{6.55}La_3Hf_{1.55}Ta_{0.45}O_{13}$ (1130 °C)	12.9330(2)	3.45×10^{-4} (22 °C/air)	0.44	48
$Li_{6.6}La_3Zr_{1.6}Sb_{0.4}O_{12}$ (1100 °C)	12.95955	7.7×10^{-4} (30 °C/air)	0.34	49
$Li_{6.625}La_3Zr_{1.625}Ta_{0.375}O_{12}$ (29 mol% Al) (cubic) (1000 °C)	12.9438	5×10^{-4} (25 °C/air)	0.41	50
$Li_{6.7}La_3Zr_{1.7}Ta_{0.3}O_{12}$ (1130 °C)	12.9721	0.96×10^{-3} (25 °C/air)	0.37	51
$Li_{6.75}La_3Zr_{1.875}Te_{0.125}O_{12}$ (1100 °C)	12.9469	3.30×10^{-4} (30 °C/air)	0.41	46
$Li_{6.75}La_3Zr_{1.75}Ta_{0.25}O_{12}$ (1050 °C co-precipitation and hot pressing method)	12.96	0.87×10^{-3} (25 °C/air)	0.22	41
$Li_{6.75}La_3Zr_{1.75}Nb_{0.25}O_{12}$ (1200 °C)	12.95	0.8×10^{-3} (25 °C/air)	0.31	52
$Li_7La_3Zr_2O_{12}$ (750 °C one-step solution method)	13.0035	2.85×10^{-6} (25 °C/air)	0.36	53
$Li_7La_3Zr_2O_{12}$ (800 °C Pechini sol–gel method, tetragonal)	a = 13.122(3) c = 12.672(3)	3.12×10^{-7} (25 °C/air)	0.67	54
$Li_7La_3Zr_2O_{12}$ (980 °C, tetragonal)	a = 13.134(4) c = 12.663(8)	1.63×10^{-6} (27 °C/air)	0.54	17
$Li_7La_3Zr_2O_{12}$ (1200 °C, sol–gel method)	12.9720	3.1×10^{-4} (25 °C/air)	0.34	55
$Li_7La_3Zr_2O_{12}$ (1050 °C hot pressing method, tetragonal)	a = 13.077(1) c = 12.715(4)	2.3×10^{-5} (25 °C/air)	0.41	56
$Li_7La_3Zr_2O_{12}$ (1230 °C)	12.9682(6)	5.11×10^{-4} (25 °C/air)	0.32	16
$Li_7La_3Zr_2O_{12}$ (1.2 wt% Al) (1200 °C polymerized complex method)	—	2×10^{-4} (25 °C/air)	—	57
$Li_7La_3Zr_2O_{12}$ (1.7 wt% Sr) (1200 °C)	12.980	5×10^{-4} (24 °C/air)	0.31	58
$Li_7La_3Zr_2O_{12}$ (CO_2 doped) (1180 °C sol–gel method)	—	5.8×10^{-4} (25 °C/air)	—	59
$Li_7La_3Zr_2O_{12}$ (CO_2 doped) (800 °C sol–gel method, tetragonal)	—	3.3×10^{-6} (25 °C/air)	—	59
$Li_7La_3Zr_2O_{12}$ (CO_2 doped) (450 °C sol–gel method)	—	1.3×10^{-6} (25 °C/air)	—	59
$Li_7La_3Zr_2O_{12}$ (0.4 mol% Ce) (1050 °C)	13.020	1.44×10^{-5} (23 °C/air)	0.48	60
$Li_7La_3Sn_2O_{12}$ (900 °C, tetragonal)	a = 13.1206(1) c = 12.5467(1)	2.6×10^{-8} (85 °C/air)	0.79	18
$Li_7La_3Hf_2O_{13}$ (1000 °C, tetragonal)	a = 13.102(6) c = 12.630(2)	9.85×10^{-7} (23 °C/air)	0.53	61
$Li_7La_3Hf_2O_{13}$ (1250 °C)	12.938(1)	2.4×10^{-4} (23 °C/air)	0.29	62
$Li_7La_3Ta_2O_{13}$ (900 °C)	12.82	3.3×10^{-6} (27 °C/air)	0.38	19
$Li_7La_3Ta_2O_{13}$ (950 °C)	12.830(4)	5.0×10^{-6} (40 °C/air)	0.55	63
$Li_7Nd_3Zr_2O_{12}$ (850 °C, tetragonal)	a = 12.9471(1) c = 12.5511(1)	4.9×10^{-7} (100 °C N_2)	0.66	64
$Li_{7.06}La_3Zr_{1.94}Y_{0.06}O_{12}$ (1200 °C)	12.9672	9.56×10^{-4} (25 °C/air)	0.29	65
$Li_{7.06}La_3Zr_{1.94}Y_{0.06}O_{12}$ (950 °C)	12.974(3)	10^{-6} (23 °C/air)	0.47	66
$Li_{7.16}La_3Zr_{1.84}Y_{0.16}O_{12}$ (950 °C)	12.995(2)	10^{-6} (23 °C/air)	0.47	66

~ extracted from the graph.

tetrahedron is connected to 4 octahedra by face sharing, as shown in Fig. 4.[23,67] If simultaneous polyhedra are occupied by Li^+ ions, then the short Li–Li distance of 2.003(2) Å seems to destabilize the structure causing the octahedral Li^+ ion to displace away from the centre of the octahedron toward the opposite side shared with an unoccupied tetrahedron. This increases the Li–Li separation from 2.003(2) Å to 2.44(2) Å.[67] Thus, it can clearly be concluded that the Li ion displacement depends on the Li occupancy of the neighboring octahedron. The fraction of displaced Li^+ ions from the center of the octahedron toward the face shared with an unoccupied tetrahedron increases linearly with increasing Li concentration, while the amount of octahedral Li displacement remains constant.[67]

The partial substitution of La and M sites in $Li_5La_3M_2O_{12}$ resulted in a change of the lattice parameters, which depend on the ionic size of the divalent ions and the sintering temperature.[11,28] With the exception of Mg ions, a direct correlation

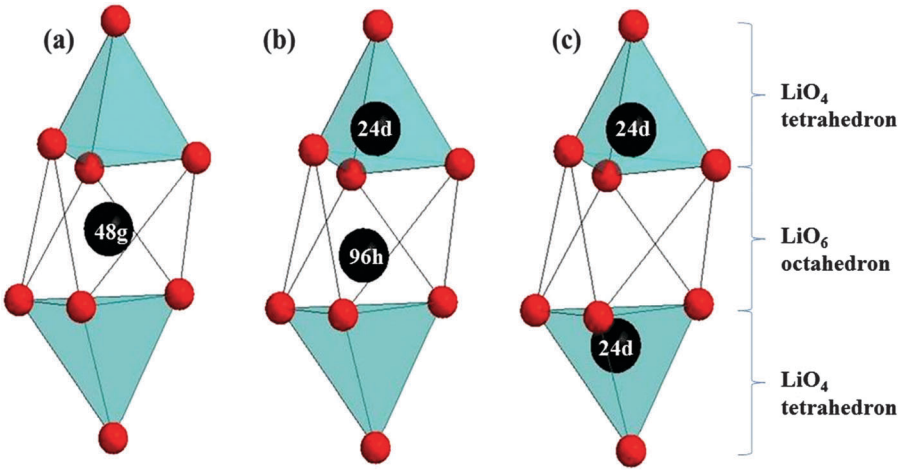

Fig. 4 Li occupancy in the garnet-type structure $Li_{5+x}La_{3-x}A_xM_{2-y}B_yO_{12}$ where A = divalent, B = tri or tetravalent and M = pentavalent ions. The following three arrangements are possible Li ion distributions (a) both tetrahedra are empty and Li^+ occupies a central position in the octahedron; (b) one Li^+ occupies a single tetrahedron shifting the octahedral Li^+ away from the shared face and (c) both tetrahedra are occupied leaving the octahedral site empty.[67]

exists between the ionic radii of the alkaline earth ions and the lattice parameters of the resulting garnet-type structure.[11] Also, the lattice parameter was found to increase with increasing sintering temperature. The small variation in the lattice parameters at different sintering temperatures was attributed to the diffusion of un-reacted metal oxides or any impurities from the surface to the bulk.[11] The lattice parameter and sintering temperature dependence seemed to have an effect on the ionic conductivity.[28]

O'Callaghan and Cussen have performed ND studies on $Li_{5+x}Ba_xLa_{3-x}Ta_2O_{12}$ (x = 0–1.6),[67] and have shown that Li in $Li_5La_3Ta_2O_{12}$ partially occupies the 24d tetrahedral site (*ca.* 80%). However, not all the Li can be accommodated and so an additional 48g octahedral site is occupied (*ca.* 14%).[23] The tetrahedral and octahedral sites are connected by a shared face (Fig. 4),[67] where simultaneous occupation results in reduced Li–Li distances. It was observed that increasing the lithium content in these garnets results in a shift from primarily tetrahedral occupancy (x = 0) to more preference for octahedral occupancy (x = 1.6), where in $Li_{6.6}Ba_{1.6}La_{1.4}Ta_2O_{12}$ the octahedral sites are filled (~57%), leaving the tetrahedral sites vacant (~14%).[67] The work of Nyman *et al.* has shown the ion-exchange reaction of $Li_5La_3M_2O_{12}$ in dilute acid, in which H^+ ions displace Li^+ ions from the garnet structure, occurs for Li in the framework tetrahedral sites, which are more populated in those compounds.[68]

2.4 $Li_7La_3M_2O_{12}$ (M = Zr, Sn) (Li_7-phases)

In 2007, Murugan *et al.* synthesized highly conductive cubic garnet-type $Li_7La_3Zr_2O_{12}$ by substitution of Zr for M in $Li_5La_3M_2O_{12}$, confirming that the garnet structure can accommodate 7 Li ions per chemical formula.[16] However, Awaka *et al.* stabilized a less conducting tetragonal polymorph with a space group $I4_1/acd$.[17] They have shown that at a sintering temperature of 980 °C, $Li_7La_3Zr_2O_{12}$ forms a less conductive tetragonal phase, instead of the highly conductive cubic phase prepared at 1230 °C (Table 1).[16] Percival *et al.* reported a similar result for $Li_7La_3Sn_2O_{12}$, where they observed the transition from tetragonal to cubic symmetry above 750 °C.[18]

Geiger *et al.* systematically studied both cubic and tetragonal phases of $Li_7La_3Zr_2O_{12}$[69] by using two different sintering methods; in the first method, the initial steps of synthesis were carried out in an Al_2O_3 crucible, while the later steps were carried out in a Pt crucible. Electron microprobe, laser ablation inductively coupled plasma mass spectrometry and Al-MAS NMR showed the presence of Al on two different Li sites in the structure. This small amount of Al is thought to have stabilized the structure in a higher conducting cubic phase compared to when this material was prepared in Pt crucible, which resulted in a less conducting tetragonal phase that transformed to the cubic phase at higher temperatures.[69] Kotobuki *et al.* reported the effect of adding Al_2O_3, as a sintering aid, for the preparation of cubic $Li_7La_3Zr_2O_{12}$. They claimed that the addition of Al_2O_3 lowered the required sintering temperature by 230 °C and suppresses the formation of the pyrochlore structure $La_2Zr_2O_7$ impurity phase, which is known to lower the Li ionic conductivity of $Li_7La_3Zr_2O_{12}$.[70]

The structural framework of the tetragonal $Li_7La_3Zr_2O_{12}$ compound was explained by Awaka *et al.* using a differential Fourier map proposing that the Li ions occupy three different sites in the $I4_1/acd$ structure, all of which are completely occupied, a key difference from the cubic garnets.[17,67] The Li(1) atoms in the tetragonal $Li_7La_3Zr_2O_{12}$ compound occupied tetrahedral 8a site; and Li(2) atoms occupied distorted octahedral (16f) sites, while the Li(3) atoms occupied distorted octahedral (32g) sites.[53] Both of these distorted octahedron had two long Li–O bonds (Li(2)–O 1.98(2) Å–2.45(2) Å and Li(3)–O: 1.89(2) Å–2.88(2) Å).[17] Similar coordination of the three lithium ion sites was reported for another tetragonal garnet, $Li_7La_3Sn_2O_{12}$, reporting that in general, one, four, and two

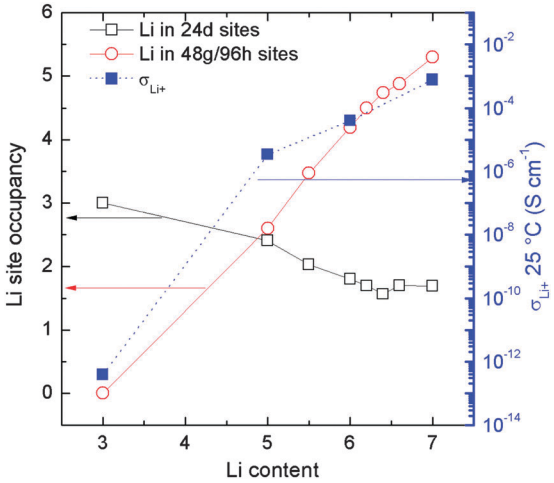

Fig. 5 Variation of Li ion occupancy[20,67,71] and room temperature conductivity as a function of Li content in the garnet structure. Total conductivity values of representative garnets as a function of Li content is also shown ($Li_3Tb_3Te_2O_{12}$ (extrapolated),[21] $Li_5La_3Ta_2O_{12}$,[8] $Li_6BaLa_2Ta_2O_{12}$[14] and $Li_7La_3Zr_2O_{12}$[16]).

Li present at the Li(1), Li(2), and Li(3) sites, respectively.[18] Fig. 5 shows the occupancy of Li ion sites as a function of Li concentration in cubic garnets.[20,67,71]

3. Li ion conductivity in garnet-like metal oxides

3.1 AC impedance studies

Li ion conduction in Li-stuffed garnet materials is commonly investigated using AC impedance spectroscopy. Fig. 6 shows a typical AC impedance plot for a Li-stuffed garnet, $Li_{6.5}La_3Nb_{1.25}Y_{0.75}O_{12}$, and a capacitive "tail" appears at low frequencies, indicating that the conductivity of the species is ionic in nature.[72] Most of the known garnets prepared by solid-state reactions exhibit mainly bulk and negligible grain-boundary contributions to the total impedance.[8,12,13,16,44–47] The relative density of the $Li_7La_3Zr_2O_{12}$ garnet was found to be in the range of about 60–98%.[56] The nature of the highly conducting grain-boundary interface layer is yet to be studied, especially for the lower density samples in order to understand the grain-boundary impedance to the total conductivity. It is also important to mention that like other known solid Li ion electrolytes, garnets are also found to undergo fast ion-exchange in water, hence the conventional Archimedes density method using water may not be very effective for density measurements. Table 1 lists the bulk Li ion conductivity and activation energy together with the cell constant and sintering temperature for known Li-garnets.[8,11–66] The Li ion conductivities of Li_3, Li_5, Li_6 and Li_7 garnets are shown in Fig. 7,[20–22] Fig. 8,[8,24,26,28,31] Fig. 9[11,13,15,21,24,26,37,40,41,43,45–52] and Fig. 10,[16,18,30,53,55,56,58–66,69] respectively.

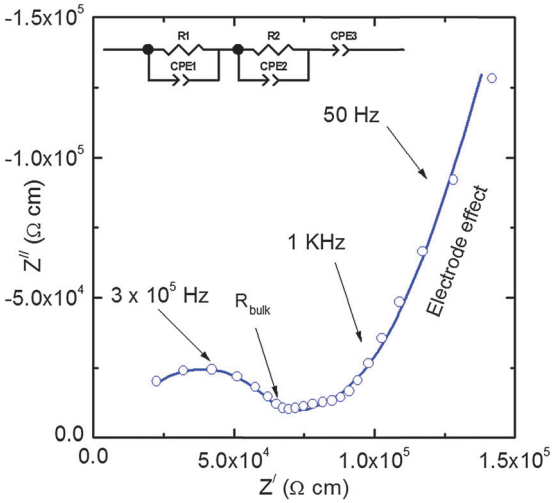

Fig. 6 Typical AC impedance plot of $Li_{6.5}La_3Nb_{1.25}Y_{0.75}O_{12}$ measured in air at −25 °C using Li-ion blocking Au electrodes.[72] The open circles represent the measured data and the solid line represents the fitted data using the equivalent circuit consisting of two parallel capacitance–resistance and capacitance contributions (shown as inset figure). The capacitive "tail" appears at the low frequency side indicating the blocking nature of mobile Li^+ ions and it is evident that the garnet-type materials are ionic conductors.[13]

Conductivity trends in garnet-type electrolytes have a very strong correlation with the Li ion concentration, which geneally increases with increasing Li ion content in Li-stuffed garnets. Ramzy and Thangadurai have shown that a simple relationship of concentration of Li^+ ions *versus* conductivity forms a near perfect linear plot for Li_5, Li_6 and Li_7 phases at room temperature.[44] In their analysis, all the Li ions are assumed to contribute to the ionic conductivity. Also, it has been shown that there is an equally linear trend for all garnet-type electrolytes for conductivity *versus* diffusion coefficient.[44] However, these trends obviously are not seen when M and La site substitutions cause a change in conductivity due to the microstructure because of sintering, density and distribution of Li^+ ion concentration at several crystallographic sites (Fig. 7–10). For $Li_5La_3Nb_2O_{12}$, Thangadurai and Weppner have reported the effect of sintering temperatures (900–1000 °C) on ionic conductivity.[28] They found that as the temperature is increased, the

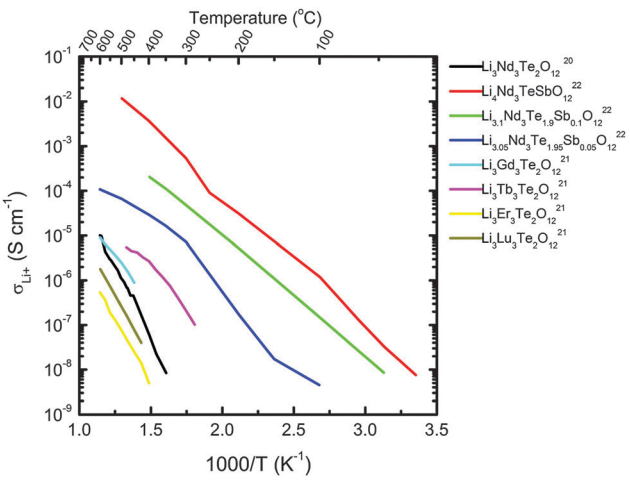

Fig. 7 Extracted Li-ion conductivity of garnet-type Li_3 phases from the literature.[20–22]

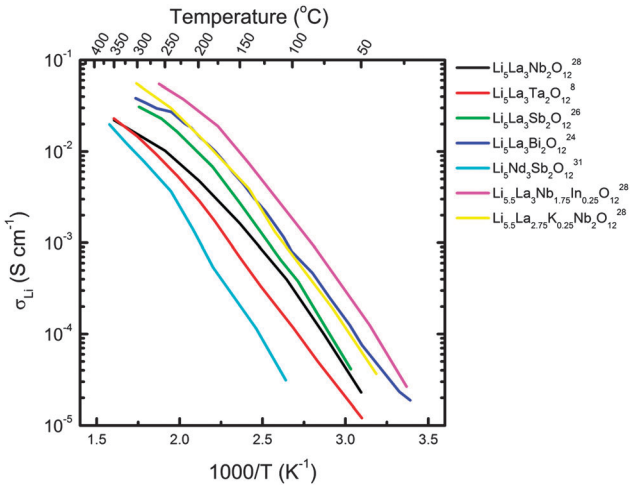

Fig. 8 Extracted Li-ion conductivity of garnet-type Li_5 and $Li_{5.5}$ phases from the literature.[8,24,26,28,31]

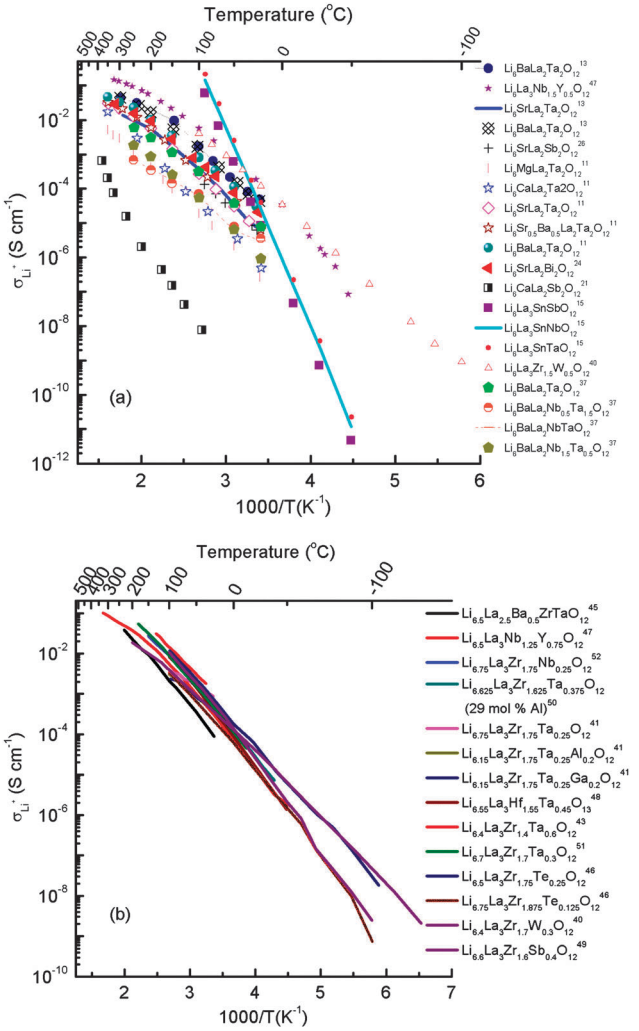

Fig. 9 Extracted Li^+ ion conductivity of garnet-type (a) Li_6 and (b) Li-excess garnets (Li_6–$Li_{6.75}$ phases) from the literature.[11,13,15,21,24,26,37,40,41,43,45–52]

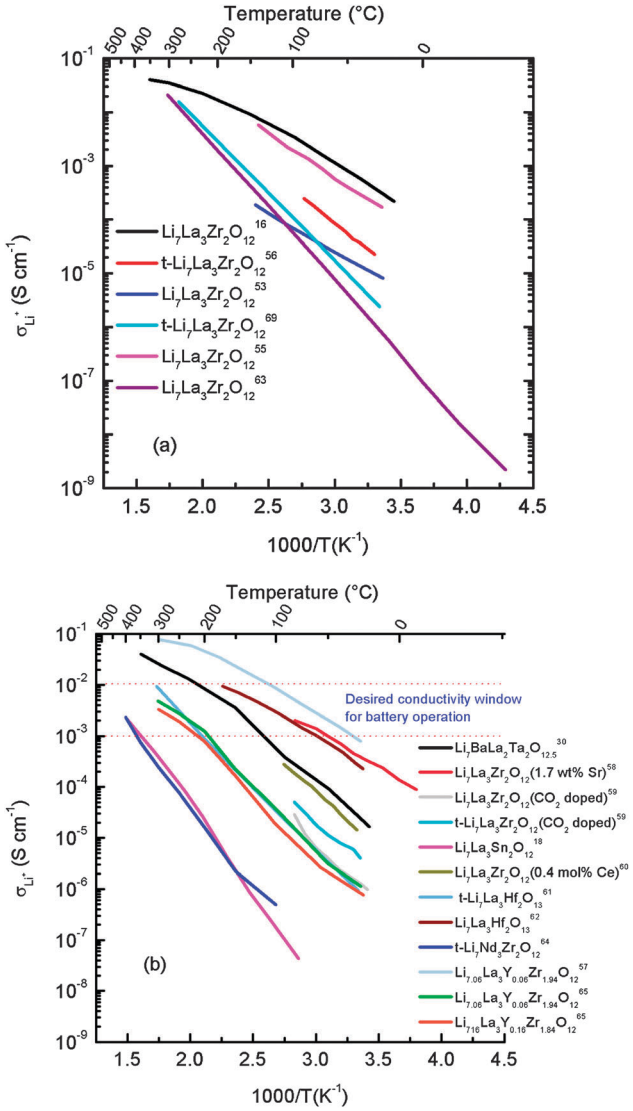

Fig. 10 Extracted Li^+ ion conductivity of Li-stuffed metal oxides with ~7 Li per chemical formula; (a) effect of polymorphs and (b) effect of doping/substitution at La or Zr sites in Li_7-phase $Li_7La_3Zr_2O_{12}$.[16,18,30,53,55,56,58–66,69]

lattice parameters decreased and the ionic conductivity increased. Similar results were reported for various garnet-type Li metal oxides (Table 1). However, data for the In- and K-doped species show an opposite effect, where the lattice parameter increased and the ionic conductivity decreased with increasing temperature.[28] This could be due to the low density of K and In-doped samples. Murugan *et al.* also found a direct correlation between sintering temperature and ionic conductivity, while an inverse correlation between activation energy and lattice expansion was realized for $Li_6CaLa_2Ta_2O_{12}$, $Li_6SrLa_2Ta_2O_{12}$, $Li_6Sr_{0.5}Ba_{0.5}La_2Ta_2O_{12}$ and $Li_6BaLa_2Ta_2O_{12}$.[11]

Murugan *et al.*[30] reported that the $x = 1$ member of $Li_{5+x}BaLa_2Ta_2O_{11.5+0.5x}$ (x = 0–2) showed a maximum bulk conductivity of 1.8×10^{-4} S cm^{-1} at 50 °C and an activation energy of 0.40 eV.[30] The lattice parameter was found to be decreasing with increasing x in $Li_{5+x}BaLa_2Ta_2O_{11.5+0.5x}$. At values $x > 1.25$, a second phase was formed in addition to the major garnet-type

phase. There is also a steep drop in the bulk and total conductivity beyond $x > 1$ in $Li_{5+x}BaLa_2Ta_2O_{11.5+0.5x}$.[30]

Percival *et al.*[73] demonstrated that Sr-doped $Li_6SrLa_2Nb_2O_{12}$ showed a higher conductivity due to the bigger ionic size compared to the corresponding Ca member. Both Sr and Ba seem to be good dopants for La in $Li_5La_3M_2O_{12}$ (M = Nb, Ta) to increase the conductivity.[12,13,73] O'Callaghan proposed that the high occupancy of Li(2) sites is very important for high lithium conductivity. The Li(2) sites are connected to each other in a 3-D fashion such that the Li^+ ions hop from one edge-shared octahedron site to another edge-shared octahedron site.[67] Percival *et al.* found that quenching the samples from higher temperatures results in enhanced low temperature conductivities.[73] Since the Li(2) site occupancy is higher at high temperatures, as shown by ND experiments, quenching the sample from 700 °C results in a higher conductivity.[73] This further provides the support for the proposed hypothesis that Li(2) site occupancy is crucial for ionic conductivity compared to Li(1) sites in Li garnet structures. An alternate explanation proposed by the same author for the high ionic conductivity in quenched samples at low temperatures involves ion trapping effects, which is a common theme in Li ion garnets.[73] The enhanced conductivity at lower temperatures was a result of decreased Li ion defect clustering and alkaline earth dopant-defect organization.

For most of the Li_6 samples, including $Li_6SrLa_2Nb_2O_{12}$[12] and $Li_6BaLa_2Ta_2O_{12}$,[13] two semicircles attributed to bulk and grain-boundary impedances at lower temperatures, while the grain-boundary contribution could not be seen at higher temperatures. It has been demonstrated that an increase in the Li ion content of the garnet structure $Li_{5+x}BaLa_2Ta_2O_{11.5+0.5x}$ (x = 0–2) decreases the grain-boundary impedance.[30] From x = 0 to x = 1 in $Li_{5+x}BaLa_2Ta_2O_{11.5+0.5x}$ the gain-boundary contribution at 50 °C decreases from 31% to 9%.[30] Another study also confirmed that the concentration of Li can have a large effect on grain-boundary impedance contributions, as shown for $Li_{5+x}Ba_xLa_{3-x}Ta_2O_{12}$ (x = 0–2).[74] At 33 °C, there is a drop in R_{gb} contributions from ~48 to ~30%, for $Li_5La_3Ta_2O_{12}$ and $Li_6BaLa_2Ta_2O_{12}$, respectively, and a proportionate increase in conductivity, while a further increase in Li content causes an increase in R_{gb} contributions.[73] It is important to note that there is a direct correlation between R_{gb} contributions and activation energy, and an inverse relationship with the lattice constant.[74]

The first known cubic $Li_7La_3Zr_2O_{12}$ exhibits a total conductivity of 7.74×10^{-4} S cm^{-1} at 25 °C which was considered to be the highest among any other family of solid lithium ion conductors and garnets.[16] The shape of the Arrhenius plots of this compound was highly reproducible, suggesting that no phase change would occur between room temperature and 350 °C. It has been suggested that this high conductivity may be due to the increased cubic lattice constant and lithium ion concentration and decreased Li^+ ion interactions with other ions in the structure. High densification, 92% of the theoretical density, might also be a reason for its improved conductivity.[16] Ohta *et al.* showed that Nb-doped $Li_{6.25}La_3Zr_{1.25}Nb_{0.75}O_{12}$ displayed a slightly higher bulk Li ion conductivity of 8×10^{-4} S cm^{-1} at 25 °C.[52]

Compared to the cubic $Li_7La_3Zr_2O_{12}$, the tetragonal polymorph shows a lower ionic conductivity by about 1–2 orders of magnitude, especially in the low temperature regime.[17,56] This discrepancy was attributed to the fact that the Li atoms and vacancies are ordered in the tetrahedral and octahedral sites, whereas these sites were very disordered in the cubic structure. Also, in the cubic analogue, an increase in the equivalent Li^+ positions due to the high symmetry of the cubic garnet resulted in an increase in the vacant Li sites on the Li-ion conduction pathway, whereas in the tetragonal structure, there was a corresponding decrease in these equivalent Li^+ positions. All these factors would result in suppressed Li^+ hopping in the tetragonal structure compared to the cubic structure, thus, lowering its Li ion conductivity.[17,56]

Recently, it was shown that the addition of Si and Al during the preparation of $Li_7La_3Zr_2O_{12}$ results in an increased total ionic conductivity, which is comparable to the bulk ionic conductivity of $Li_7La_3Zr_2O_{12}$ without the addition of Si and Al.[75] It has been proposed that Si and Al addition resulted in the formation of an amorphous Li–Al–Si–O/$LiAlSiO_4$ interface, which effectively removed the grain-boundary resistance by facilitating Li^+ ion movement between the particles.[75]

3.2 Direct current method

The electronic conductivity (σ_e) due to total electrical conductivity was determined using the DC polarization method employing 'inert' Au and Li reversible electrodes. The Li ion transference number was found to be close to that for $Li_6La_2BaTa_2O_{12}$ and $Li_7La_3Zr_2O_{12}$ (LLZ) at unit Li activity.[13,16] Similar results were reported for Al, Nb-doped $Li_7La_3Zr_2O_{12}$.[52] The Al-doped $Li_7La_3Zr_2O_{12}$ showed a very low electronic conductivity of 2×10^{-8} S cm^{-1} at room temperature.[76] The Li ion charge transfer resistance (CTR) was obtained using symmetrical Li electrodes for $Li_7La_3Zr_2O_{12}$.[50,75,77–79] The CTR of the symmetrical cell Li/LLZ/Li was found to be in the range 1.1–5.5 kΩ at room temperature.[77] This difference in CTR may have been caused by the poor wettability of Li with $Li_7La_3Zr_2O_{12}$ and by the formation of interface layers on the Li surface due to contamination. It has been suggested that thin and dense LLZ with a uniform surface appear to be desired for high current density application.[77] A CTR of 20.4 kΩ at room temperature was obtained for a LLZ pellet with dimensions of 5.3 mm diameter and 16.2 mm thickness.[78]

4. The Li ion conduction mechanism in Li garnets

O'Callaghan and Cussen performed an in-depth ND study on $Li_{5+x}Ba_xLa_{3-x}Ta_2O_{12}$ ($0 < x \leq 1.6$) to understand Li ion occupancy at octahedral and tetrahedral sites and its relationship with the conduction. They started by establishing an unusually high displacement parameter for the tetrahedral site in the x = 1 member, as compared to other garnets.[67] Using variable temperature NMR, they showed that no change

occurred in the Li distribution of the $x = 1$ member, which indicates that the displacement of Li in octahedral and tetrahedral sites is due to static disorder rather than dynamic processes.[67] Since each tetrahedron is face sharing to four octahedra and each octahedron is face sharing to two tetrahedra by opposing faces, displacement away from any neighbor would be a shift towards a differing neighboring Li (Fig. 4).[67] But, should a neighboring Li site be empty, the displacement would cause the Li–Li distance between neighboring octahedral/tetrahedral sites to change from 2.003(2) Å to 2.44(2) Å.[67] This shows that only two of the three neighboring tetrahedral–octahedral–tetrahedral sites can be occupied, to allow sufficient Li–Li spacing.[67] To show the significance of the octahedral site on conductivity, they found that as x increases to 1.6, there is a large displacement 57(2)% of Li ion in the octahedral site. A significant destabilizing effect on the Li in these sites is responsible for the extremely high mobility in the structure.[67]

4.1 Solid state Li NMR

In an Li_3 compound, such as $Li_3Nd_3Te_2O_{12}$, the ^{6}Li NMR studies showed just one set of resonance corresponding to ordered arrangement of Li^+ ions in the tetrahedral sites only coupled with the paramagnetic Nd^{3+}.[22] On the other hand, Li_5, Li_6 and Li_7 garnet phases appeared to show another set of resonances, corresponding to the presence of Li(2) sites on the distorted octahedral sites (48g).[9] This second set of resonance was observed to increase in area with increasing Li ion concentration.[9] The partially occupied tetrahedral (24d) sites in Li rich compounds did not show any difference in the ^{6}Li NMR experiments compared to the Li_3 compounds. O'Callaghan *et al.* did not observe Li^+ ion movement or hopping between Li(1) and Li(2) sites.[22] This suggests that even in Li^+ rich compounds, the partially occupied Li^+ tetrahedral sites do not seem to be involved in the Li^+ ion conduction. It is the Li^+ ion distorted octahedral sites which are highly mobile and are involved in the hopping from one edge shared oxide octahedron to another, resulting in high Li^+ ion conductivity.

Another extensive solid-state ^{7}Li NMR study by Wullen *et al.* reported that increasing the final annealing temperature of the $Li_5La_3Nb_2O_{12}$ compound increases the ionic conductivity due to increasing occupancy at the octahedral sites.[80] This correlation suggests that the Li residing in these sites are mobile and are responsible for high ionic conduction. This was further supported by a higher jump rates for Li at the octahedral sites compared to that of the tetrahedral sites. Samples prepared at 850 °C only showed appreciable Li mobility at 77 °C, while sample sintered at 900 °C exhibited high Li ion mobility at ambient temperature.[80] In the 850 °C prepared $Li_5La_3Nb_2O_{12}$ sample 60% of Li was present in the tetrahedral sites, but only 16% was found in the 900 °C prepared sample.[80] Since a maximum of 3 Li ions can occupy the tetrahedral sites, one can therefore assume the complete occupation of the tetrahedral sites, while the remaining 2 Li ions occupy the octahedral sites. Meanwhile, there is a 2/3 vacancy of the tetrahedral sites in the 900 °C prepared sample.[80] They also showed that over a temperature range of 63–137 °C, the width of the tetrahedral peak remained unchanged, indicating less mobility of the ions in the tetrahedral sites. 2D exchange NMR at a mixing time of 1 s also suggest a fast exchange from one octahedral site to another[80] which is in corroboration with Thangadurai *et al.*, who suggested the jump of Li ions merely between octahedral sites.[8] Koch and Vogel believed that this does not necessarily indicate that Li in the tetrahedral sites are immobile, but rather seems to be less mobile.[81] However, further work is required to fully understand the absolute contribution of these two different sites to the total Li-ion conductivity.

4.2 Computational method

In an early work, Thangadurai *et al.* first studied the Li ion conduction in $Li_5La_3M_2O_{12}$ (M = Nb, Ta) using a computational calculation involving bond valence sum (BVS) analysis. They have shown that Li ion conduction is anisotropic and occurs around the MO_6 octahedron.[82] They have shown that BVS of metal ions in $Li_5La_3M_2O_{12}$ was found to be rather unusual for the original single-crystal data and optimized the position of light atoms, especially oxygen and Li ions using the ''global instability index,'' and the chemical plausibility of the structure model using a bond valence mismatch minimization procedure.[82] Internal friction investigations done on cubic $Li_7La_3Ta_2O_{13}$ by Wang *et al.* revealed a prominent peak at 7 °C, comprised of two sub-peaks P1 and P2, suggesting a possible mechanism of lithium ion diffusion between the tetrahedral 24d site and the octahedral 48g site and between the octahedral 48g sites.[19] Thus, the proposed Li ion conduction mechanism seems to be highly dependent on the chemical composition of the garnets.

Ab initio tools, based on density functional theory (DFT), were used by Xu *et al.* to study three different garnet-type cubic structures such as $Li_3La_3Te_2O_{12}$, $Li_5La_3Nb_2O_{12}$ and $Li_7La_3Zr_2O_{12}$.[83] The analysis suggests that the Li_3 and Li_5 phases have high Li occupancy in the tetrahedral sites (24d) in the garnet-like structure with the space group $Ia\bar{3}d$.[83] In the Li_3 compound, all the Li ions occupy the tetrahedral sites (24d), therefore, the only possible migration path is from the tetrahedral site to the octahedral site (48g/96h) with an activation energy of 1.5 eV which is found to be comparable to the experimental value of 1.2 eV.[20] In $Li_5La_3Nb_2O_{12}$, Li ions occupy the tetrahedral sites (24d) and one third of the octahedral sites (48g/96h), therefore Li ion transport is now possible between the filled octahedral sites (48g/96h) and the vacant octahedral sites (48g/96h), bypassing the tetrahedral site (24d).[83] In contrast, in the $Li_7La_3Zr_2O_{12}$ phase, the occupancy of tetrahedral sites is reduced (only $\sim$50%) and Li occupancy in the octahedral sites increased to 90%; now Li ions can move from one octahedral site (48g/96h), through the tetrahedral site (24d) to the adjacent vacant octahedral site (48g/96h). This DFT study also clearly suggests that the bulk ionic conductivity of Li garnets is likely to be solely dependent on the Li concentration, and the effect of dopants on the garnet conductivity appears to be minor.[83] Also, conduction pathways seem to be highly correlated to the Li content in the Li-stuffed garnets.

5. Chemical stability and compatibility with Li cathodes

The chemical compatibility of $Li_5La_3Bi_2O_{12}$ with different Li cathodes was analyzed by Gao *et al.*[25] $Li_5La_3Bi_2O_{12}$ and Li cathode material were mixed (1 : 1 wt%) and heated for 24 h in air at 300–600 °C. The phase composition was examined by PXRD. For $LiCoO_2$, peaks for both individual phases were present without any new phases being formed, indicating that the two materials are stable up to 600 °C. However, for $LiMn_2O_4$, a new phase $Bi_2La_4O_9$ was observed in the spectrum after heating at 400 °C. When heated to 600 °C, peaks corresponding to garnet-type $Li_5La_3Bi_2O_{12}$ were no longer observed; therefore, these materials are not compatible with one another at 600 °C. PXRD studies showed that $Li_6BaLa_2Ta_2O_{12}$ was found to be chemically stable and compatible with $LiCoO_2$ up to 400 °C.[84]

The thermal stability of cubic $Li_7La_3Zr_2O_{12}$ was confirmed *via* thermo-gravimetric and differential thermal analysis (TG-DTA). Over the heating and cooling cycles in TG-DTA, no major weight loss or phase transition was detected from 20–900 °C. This compound was also found to be chemically stable against the reaction with molten lithium, and ambient air for long periods of time.[16] However, when a thin film of $LiCoO_2$ was applied on $Li_7La_3Zr_2O_{12}$ (LLZ), formation of an intermediate reaction layer was observed, which lowered the electrochemical performance.[85] Solid-state Li/LLZ/Li and $LiCoO_2$/LLZ/Li cells were successfully operated showing reversible charge–discharge behavior; however, $LiCoO_2$/LLZ/Li showed high interfacial resistance and low cycle capacity.[77]

6. Proton-exchange in garnets under humidity and water

Nyman *et al.* first described a Li^+/H^+ ion-exchange reaction for $Li_5La_3M_2O_{12}$ (M = Nb, Ta) garnets, for the purpose of vacating the non-mobile, tetrahedral Li sites.[68] An acidic exchange was also performed by adding 1 M HNO_3 solution. The solid-state Li NMR study suggested that it was the Li ions in the tetrahedral sites that were exchanged.[68] As the Li content is increased in $Li_5La_3M_2O_{12}$ and more Li ions occupy octahedral positions, it is believed that the proton exchange would proceed to a lesser extent.[86–88]

The chemical stability of various Li_7 tetragonal phases has also been studied in acids, water and aqueous LiCl and LiOH. The cubic $Li_7La_3Zr_2O_{12}$ garnet has shown stability in various aqueous solutions including 0.1 M HCl, 1 M LiOH, saturated LiCl, and distilled H_2O after treatment at 50 °C for one week.[87] There was an evident change in surface morphology of the garnet for the HCl and LiOH solutions. The conductivity of the products following chemical stability treatment was measured and showed no change after aqueous LiCl treatment; however, a significant decrease in conductivity was observed after treatment in water. It is possible that a Li^+/H^+ ion-exchange reaction may have occurred with the water treatment. The reversible nature of the Li^+/H^+ ion-exchange reaction was investigated using a saturated $LiNO_3$ solution.[87] Galven *et al.* presented a structural study on $Li_7La_3Sn_2O_{12}$ using Li^+/H^+ ion-exchange.[89] The proton-exchange reaction was performed using a benzoic acid and ethanol solution which was heated under reflux for one week. They also noted that the ion exchange occurs in a humid air environment as well. Although, the garnet structure was maintained, the tetragonal phase was lost and the product was cubic garnet-type phase, similar to other Li_5 and Li_6 compounds. Like other studies, it was found that the proton-exchange reaction could not be completed in water, ~80% in $Li_5La_3M_2O_{12}$ to give the H analogue.[68,87] Further studies on the effect of particle size on proton-exchange in Li-stuffed garnet are required to fully understand the ion-exchange capacity.

7. Conclusions

The current research on Li-stuffed garnet-type structured materials leads to the following key conclusions:

- the garnet structure can accommodate a minimum of three Li ions and a maximum of ~seven Li ions per chemical formula;
- the Li ion conductivity increases with increasing Li content in the garnet structure, and the optimum concentration of Li ions for maximum conductivity was found to be in the range ~6.5 to 7. However, sintering temperature and potential impurity phases seem to be very critical in controlling the Li ion conductivity; the garnet with the nominal chemical formula $Li_{6.4}La_3Zr_{1.4}Ta_{0.6}O_{12}$, prepared at 1140 °C, exhibits the highest bulk conductivity of 10^{-3} S cm^{-1} at room temperature;
- divalent Ba ions substitution for La site and tetravalent Zr substitution for pentavalent in Nb/Ta site seem to be the best approach to increase the conductivity of the parent phase $Li_5La_3M_2O_{12}$ (M = Nb, Ta);
- solid state Li NMR and computational studies support that the Li conduction mechanism occurs mostly between the octahedral sites and Li in these sites are connected to each other in a 3-D fashion such that the ions can hop from one edge shared octahedron to another and also, Li ion conduction pathways appear to be correlated to the Li concentration in garnets;
- solely Zr and Ta based Li garnets are stable against chemical reaction with elemental Li and showed electrochemical stability up to 6 V per Li at room temperature;
- the highly conducting cubic $Li_7La_3Zr_2O_{12}$ phase was stabilized by intrinsic Al-doping at elevated temperatures from the reaction containers used for preparation, while the low-temperature synthesized "Al-free" cubic $Li_7La_3Zr_2O_{12}$ phase showed about 2 orders of magnitude lower bulk conductivity at low temperatures;
- like other fast alkali ion conductors Li-rich garnets undergo fast proton-exchange in water, dilute acids, and aqueous LiCl/LiOH solutions and the exchange seems to be favored at the tetrahedral sites. $Li_5La_3M_2O_{12}$ undergoes ion-exchange more readily compared to Li-rich Li_6 and Li_7 phases under comparable experimental conditions.

Acknowledgements

This work was supported by the Natural Sciences and Engineering Research Council of Canada (NSERC) through the Discovery

Grants (DG). V.T. also thanks Adam Ramzy, Tania Pannu, and Lina Troung who have contributed in the development of solid Li ion electrolytes and for their input to this review paper.

References

1 J. M. Tarascon and M. Armand, *Nature*, 2001, **414**, 359–367.
2 A. D. Robertson, A. R. West and A. G. Ritchie, *Solid State Ionics*, 1997, **104**, 1–11.
3 G. Y. Adachi, N. Imanaka and H. Aono, *Adv. Mater.*, 1996, **8**, 127–135.
4 V. Thangadurai and W. Weppner, *Ionics*, 2006, **12**, 81–92.
5 S. Stramare, V. Thangadurai and W. Weppner, *Chem. Mater.*, 2003, **15**, 3974–3990.
6 F. Abbattista, M. Vallino and D. Mazza, *Mater. Res. Bull.*, 1987, **22**, 1019–1027.
7 H. Hyooma and K. Hayashi, *Mater. Res. Bull.*, 1988, **23**, 1399–1407.
8 V. Thangadurai, H. Kaack and W. Weppner, *J. Am. Ceram. Soc.*, 2003, **86**, 437–440.
9 E. J. Cussen, *J. Mater. Chem.*, 2010, **20**, 5167–5173.
10 A. F. Wells, *Structural Inorganic Chemistry*, Clarendon Press, Oxford, 4th edn, 1975.
11 R. Murugan, V. Thangadurai and W. Weppner, *J. Electrochem. Soc.*, 2008, **155**, A90–A101.
12 V. Thangadurai and W. Weppner, *J. Am. Ceram. Soc.*, 2005, **88**, 411–418.
13 V. Thangadurai and W. Weppner, *Adv. Funct. Mater.*, 2005, **15**, 107–112.
14 J. Awaka, N. Kijima, Y. Takahashi, H. Hayakawa and J. Akimoto, *Solid State Ionics*, 2009, **180**, 602–606.
15 H. Xie, Y. Li, J. Han, Y. Dong, M. P. Paranthaman, L. Wang, M. Xu, A. Gupta, Z. Bi, C. A. Bridges, M. Nakanishi, A. P. Sokolov and J. B. Goodenough, *J. Electrochem. Soc.*, 2012, **159**, A1148–A1151.
16 R. Murugan, V. Thangadurai and W. Weppner, *Angew. Chem., Int. Ed.*, 2007, **46**, 7778–7781.
17 J. Awaka, N. Kijima, H. Hayakawa and J. Akimoto, *J. Solid State Chem.*, 2009, **182**, 2046–2052.
18 J. Percival, E. Kendrick, R. I. Smith and P. R. Slater, *Dalton Trans.*, 2009, 5177–5181.
19 W. G. Wang, X. P. Wang, Y. X. Gao and Q. F. Fang, *Solid State Ionics*, 2009, **180**, 1252–1256.
20 M. P. O'Callaghan, D. R. Lynham, E. J. Cussen and G. Z. Chen, *Chem. Mater.*, 2006, **18**, 4681–4689.
21 E. J. Cussen, T. W. S. Yip, G. O'Neill and M. P. O'Callaghan, *J. Solid State Chem.*, 2011, **184**, 470–475.
22 M. P. O'Callaghan, A. S. Powell, J. J. Titman, G. Z. Chen and E. J. Cussen, *Chem. Mater.*, 2008, **20**, 2360–2369.
23 E. J. Cussen, *Chem. Commun.*, 2006, 412–413.
24 R. Murugan, W. Weppner, P. Schmid-Beurmann and V. Thangadurai, *Mater. Sci. Eng., B*, 2007, **143**, 14–20.
25 Y. X. Gao, X. P. Wang, W. G. Wang, Z. Zhuang, D. M. Zhang and Q. F. Fang, *Solid State Ionics*, 2010, **181**, 1415–1419.
26 R. Murugan, W. Weppner, P. Schmid-Beurmann and V. Thangadurai, *Mater. Res. Bull.*, 2008, **43**, 2579–2591.
27 E. J. Cussen and T. W. S. Yip, *J. Solid State Chem.*, 2007, **180**, 1832–1839.
28 V. Thangadurai and W. Weppner, *J. Solid State Chem.*, 2006, **179**, 974–984.
29 I. P. Roof, M. D. Smith, E. J. Cussen and H. zur Loye, *J. Solid State Chem.*, 2009, **182**, 295–300.
30 R. Murugan, V. Thangadurai and W. Weppner, *Appl. Phys. A: Mater. Sci. Process.*, 2008, **91**, 615–620.
31 J. Percival, E. Kendrick and P. R. Slater, *Mater. Res. Bull.*, 2008, **43**, 765–770.
32 H. Peng, Q. Wu and L. Xiao, *J. Sol–Gel Sci. Technol.*, 2013, **66**, 175–179.
33 S. Narayanan and V. Thangadurai, *J. Power Sources*, 2011, **196**, 8085–8090.
34 Y. X. Gao, X. P. Wang, W. G. Wang and Q. F. Fang, *Solid State Ionics*, 2010, **181**, 33–36.
35 M. Kotobuki and K. Kanamura, *Ceram. Interfaces*, 2013, **39**, 6481–6487.
36 M. A. Howard, O. Clemens, E. Kendrick, K. S. Knight, D. C. Apperley, P. A. Anderson and P. R. Slater, *Dalton Trans.*, 2012, **41**, 12048–12053.
37 Y. Zhong, Q. Zhou, Y. Guo, Z. Li and Y. Qiang, *Ionics*, 2013, **19**, 697–700.
38 I. Kokal, K. V. Ramanujachary, P. H. L. Notten and H. T. Hintzen, *Mater. Res. Bull.*, 2012, **47**, 1932–1935.
39 Y. Li, C. Wang, H. Xie, J. Cheng and J. B. Goodenough, *Electrochem. Commun.*, 2011, **13**, 1289–1292.
40 L. Dhivya, N. Janani, B. Palanivel and R. Murugan, *AIP Adv.*, 2013, **3**, 082115.
41 J. L. Allen, J. Wolfenstine, E. Rangasamy and J. Sakamoto, *J. Power Sources*, 2012, **206**, 315–319.
42 J. Wolfenstine, J. Ratchford, E. Rangasamy, J. Sakamoto and J. L. Allen, *Mater. Chem. Phys.*, 2012, **134**, 571–575.
43 Y. Li, J. Han, C. Wang, H. Xie and J. B. Goodenough, *J. Mater. Chem.*, 2012, **22**, 15357–15361.
44 A. Ramzy and V. Thangadurai, *ACS Appl. Mater. Interfaces*, 2010, **2**, 385–390.
45 S. Narayanan, V. Epp, M. Wilkening and V. Thangadurai, *RSC Adv.*, 2012, **2**, 2553–2561.
46 C. Deviannapoorani, L. Dhivya, S. Ramakumar and R. Murugan, *J. Power Sources*, 2013, **240**, 18–25.
47 S. Narayanan, F. Ramezanipour and V. Thangadurai, *J. Phys. Chem. C*, 2012, **116**, 20154–20162.
48 A. Gupta, R. Murugan, M. P. Paranthaman, Z. Bi, C. A. Bridges, M. Nakanishi, A. P. Sokolov, K. S. Han, E. W. Hagaman, H. Xie, C. B. Mullins and J. B. Goodenough, *J. Power Sources*, 2012, **209**, 184–188.
49 S. Ramakumar, L. Satyanarayana, S. V. Manorama and R. Murugan, *Phys. Chem. Chem. Phys.*, 2013, **15**, 11327–11338.
50 H. Buschmann, S. Berendts, B. Mogwitz and J. Janek, *J. Power Sources*, 2012, **206**, 236–244.
51 Y. Wang and W. Lai, *Electrochem. Solid-State Lett.*, 2012, **15**, A68–A71.

52 S. Ohta, T. Kobayashi and T. Asaoka, *J. Power Sources*, 2011, **196**, 3342–3345.
53 H. Xie, Y. Li and J. B. Goodenough, *Mater. Res. Bull.*, 2012, **47**, 1229–1232.
54 I. Kokal, M. Somer, P. H. L. Notten and H. T. Hintzen, *Solid State Ionics*, 2011, **185**, 42–46.
55 Y. Li, J. Han, C. Wang, S. C. Vogel, H. Xie, M. Xu and J. B. Goodenough, *J. Power Sources*, 2012, **209**, 278–281.
56 J. Wolfenstine, E. Rangasamy, J. L. Allen and J. Sakamoto, *J. Power Sources*, 2012, **208**, 193–196.
57 Y. Jin and P. J. McGinn, *J. Power Sources*, 2011, **196**, 8683–8687.
58 A. Dumon, M. Huang, Y. Shen and C. Nan, *Solid State Ionics*, 2013, **243**, 36–41.
59 S. Toda, K. Ishiguro, Y. Shimonishi, A. Hirano, Y. Takeda, O. Yamamoto and N. Imanishi, *Solid State Ionics*, 2013, **233**, 102–106.
60 E. Rangasamy, J. Wolfenstine, J. Allen and J. Sakamoto, *J. Power Sources*, 2013, **230**, 261–266.
61 J. Awaka, N. Kijima, K. Kataoka, H. Hayakawa, K. Ohshima and J. Akimoto, *J. Solid State Chem.*, 2010, **183**, 180–185.
62 T. Zaiss, M. Ortner, R. Murugan and W. Weppner, *Ionics*, 2010, **16**, 855–858.
63 C. R. Mariappan, K. I. Gnanasekar, V. Jayaraman and T. Gnanasekaran, *J. Electroceram.*, 2013, **30**, 258–265.
64 M. Howard, O. Clemens, K. Knight, P. Anderson, S. Hafiz, P. M. Panchmatia and P. Slater, *J. Mater. Chem. A*, 2013, **1**, 14013–14022.
65 R. Murugan, S. Ramakumar and N. Janani, *Electrochem. Commun.*, 2011, **13**, 1373–1375.
66 G. T. Hitz, E. D. Wachsman and V. Thangadurai, *J. Electrochem. Soc.*, 2013, **160**, A1248–A1255.
67 M. P. O'Callaghan and E. J. Cussen, *Chem. Commun.*, 2007, 2048–2050.
68 M. Nyman, T. M. Alam, S. K. McIntyre, G. C. Bleier and D. Ingersoll, *Chem. Mater.*, 2010, **22**, 5401–5410.
69 C. A. Geiger, E. Alekseev, B. Lazic, M. Fisch, T. Armbruster, R. Langner, M. Fechtelkord, N. Kim, T. Pettke and W. Weppner, *Inorg. Chem.*, 2011, **50**, 1089–1097.
70 M. Kotobuki, K. Kanamura, Y. Sato and T. Yoshida, *J. Power Sources*, 2011, **196**, 7750–7754.
71 H. Xie, J. A. Alonso, Y. Li, M. T. Fernandez-Diaz and J. B. Goodenough, *Chem. Mater.*, 2011, **23**, 3587–3589.
72 S. Narayanan, *Development of Novel Garnet-Type Solid Electrolytes for Potential Application in Li Ion Batteries*, MSc thesis, Department of Chemistry, University of Calgary, 2012.
73 J. Percival, D. Apperley and P. R. Slater, *Solid State Ionics*, 2008, **179**, 1693–1696.
74 R. Murugan, V. Thangadurai and W. Weppner, *Ionics*, 2007, **13**, 195–203.
75 S. Kumazaki, Y. Iriyama, K. Kim, R. Murugan, K. Tanabe, K. Yamamoto, T. Hirayama and Z. Ogumi, *Electrochem. Commun.*, 2011, **13**, 509–512.
76 E. Rangasamy, J. Wolfenstine and J. Sakamoto, *Solid State Ionics*, 2012, **206**, 28–32.
77 M. Kotobuki, H. Munakata, K. Kanamura, Y. Sato and T. Yoshida, *J. Electrochem. Soc.*, 2010, **157**, A1076–A1079.
78 H. Buschmann, J. Dolle, S. Berendts, A. Kuhn, P. Bottke, M. Wilkening, P. Heitjans, A. Senyshyn, H. Ehrenberg, A. Lotnyk, L. Kienle and J. Janek, *Phys. Chem. Chem. Phys.*, 2011, **13**, 19378–19392.
79 H. El Shinawi and J. Janek, *J. Power Sources*, 2013, **225**, 13–19.
80 L. van Wullen, T. Echelmeyer, H. Meyer and D. Wilmer, *Phys. Chem. Chem. Phys.*, 2007, **9**, 3298–3303.
81 B. Koch and M. Vogel, *Solid State Nucl. Magn. Reson.*, 2008, **34**, 37–43.
82 V. Thangadurai, S. Adams and W. Weppner, *Chem. Mater.*, 2004, **16**, 2998–3006.
83 M. Xu, M. S. Park, J. M. Lee, T. K. Kim, Y. S. Park and E. Ma, *Phys. Rev. B: Condens. Matter Mater. Phys.*, 2012, **85**, 052301.
84 V. Thangadurai and W. Weppner, *J. Power Sources*, 2005, **142**, 339–344.
85 K. H. Kim, Y. Iriyama, K. Yamamoto, S. Kumazaki, T. Asaka, K. Tanabe, C. A. J. Fisher, T. Hirayama, R. Murugan and Z. Ogumi, *J. Power Sources*, 2011, **196**, 764–767.
86 Y. Shimonishi, A. Toda, T. Zhang, A. Hirano, N. Imanishi, O. Yamamoto and Y. Takeda, *Solid State Ionics*, 2011, **183**, 48–53.
87 L. Troung and V. Thangadurai, *Chem. Mater.*, 2011, **23**, 3970–3977.
88 L. Truong and V. Thangadurai, *Inorg. Chem.*, 2012, **51**, 1222–1224.
89 C. Galven, J. Fourquet, M. Crosnier-Lopez and F. Le Berre, *Chem. Mater.*, 2011, **23**, 1892–1900.